frontiers | Frontiers in Energy Research

TYPE Original Research
PUBLISHED 04 October 2024
DOI 10.3389/fenrg.2024.1428524

OPEN ACCESS

EDITED BY
Chenghong Gu,
University of Bath, United Kingdom

REVIEWED BY
Runze Wu,
North China Electric Power University, China
Fan Chen,
Nanjing Institute of Technology (NJIT), China
Roberto Francisco Coelho,
Federal University of Santa Catarina, Brazil

*CORRESPONDENCE
Qunying Liu,
lqy1206@126.com

RECEIVED 06 May 2024
ACCEPTED 11 September 2024
PUBLISHED 04 October 2024

CITATION
Chen Z, Hao Z, An J, Fan W, Huang Y and Liu Q (2024) Research on a coordinated control strategy of three-phase photovoltaic converters based on a buck–boost DC link. *Front. Energy Res.* 12:1428524. doi: 10.3389/fenrg.2024.1428524

Research on a coordinated control strategy of three-phase photovoltaic converters based on a buck–boost DC link

Zhiyong Chen[1], Zhifang Hao[1], Jiakun An[1], Wenyi Fan[1], Yuan Huang[1] and Qunying Liu[2]*

[1]Economic and Technical Research Institute of State Grid Hebei Electric Power Co., Ltd., Shijiazhuang, China, [2]School of Automation Engineering, University of Electronic Science and Technology of China, Chengdu, China

The high inductance current ripple and the PV voltage fluctuations limitation at the DC (direct current) -DC link have been the unsolved problems in the photovoltaic systems tied in grid. A control strategy with a current hysteresis loop is proposed to address the issues of high inductance current ripple in photovoltaic systems which can achieve real-time duty cycle regulation. Differing from the conventional mode that uses one switch in the buck–boost DC–DC link, two switches have been designed here to separate the buck and boost modes for the coordinated control, which can achieve a wide PV voltage fluctuations range. Based on the conventional fixed-duty cycle determination method, a real-time duty cycle determination method is proposed by introducing changes in inductance current. In order to improve power conversion efficiency, the incremental conductance method is improved by introducing the steepest gradient descent to quickly achieve the maximum power point tracking. This study experimentally verifies the proposed current hysteresis coordinated control method, effectively suppressing the ripple of the inductor current and expand the PV voltage fluctuation in the DC–DC link on the basis of maintaining power conversion efficiency as much as possible.

KEYWORDS

photovoltaic panel, coordinated control strategy, current hysteresis loop control, buck-boost circuit, DC-DC link

1 Introduction

In the last 20 years, many studies have focused on the topology of DC–DC links and converter technology for the DC–AC interface of photovoltaic (PV) cells and the grid. DC–AC interface technology has included voltage source converters (VSIs) adapted for the interface of PV panels with the grid (Teodorescu et al., 2011). To address the constraint of low leakage current for non-isolated grid-tied converters, a series of different converter structures and control schemes have been investigated (Alluhaybi et al., 2020; Khan et al., 2020), some considering stochasticity (Nan et al., 2018). In addition to converter configuration reformation, the topology and control strategy of the DC–DC link is also a key area of improvement for less harmonics and higher transferring efficiency. Liao et al. (2017) proposed a novel PV converter with a PV current decoupling strategy which can achieve maximum power point tracking performance without increasing electrolyte capacitance. The current decoupling tank in the proposed PV converter can buffer the

difference between the DC current generated by the PV panel and the rectified sinusoidal AC of the power grid. Mohammadi et al. (2018) proposed a novel switching frequency modulation method to address the trade-off between voltage gain and voltage harmonics caused by the coupling of the duty cycle and modulation ratio. Ho and Siu (2019) proposed a new converter structure in which high-frequency switches are used to control the inductor current, while low-frequency switches form a filter structure that adapts to different operating conditions. Unfortunately, the designed structure led to more energy loss.

The output voltage of PV panels is often affected by ambient factors such as sunlight intensity, temperature, and shadow. A buck–boost converter is required to adapt to a wide range of DC voltage fluctuations. Callegaro et al. (2019) proposed a single-phase, single-stage buck–boost converter which uses five switches (implemented using MOSFET power with external fast recovery diodes) to provide buck–boost operation for the wide range of changes in PV output voltage while eliminating leakage current. In order to improve power extraction under the ambient condition, a buck–boost single-phase transformer-free grid-connected photovoltaic converter based on coupled inductance has been proposed by Kumar and Singh (2019) and Hafiz et al. (2021) which has the ability to extract maximum power from the series of photovoltaic panels. Dutta and Chatterjee (2018) proposed a day-and-night operational single-phase energy stored quasi-Z-source-cascaded H-bridge (ES-qZS-CHB) converter PV system to solve the active and reactive power control problem. They designed optimal multiple combinations of duty cycle and modulation ratio to achieve the same voltage gain during night operation.

In order to balance the output voltage of input-independent-output series modules, bidirectional buck–boost and LC series power balancing units have been proposed for multiple PV panels by Dutta and Chatterjee (2020). Liang et al. (2021) proposed a multi-PV panel with battery and bidirectional converter interconnected with a three-phase grid. A buck–boost converter is connected to the main VSC with BES is responsible for the load level adjusting and the MPPT voltage. A new solar PV-fed dynamic voltage restorer (DVR) based on a trans-Z-source converter was proposed by Huang et al. (2021) to improve the power quality of on-grid PV systems, in which a hybrid unit vector template with maximum constant boost control method was proposed for transZSI-DVR. Chauhan et al. (2021) outlined an integrated three-phase transformer-less PV converter structure which utilizes an interleaved dual output buck–boost converter to obtain the boosting voltage. From a single PV source, the voltage waveform of the output terminal can be synthesized into three levels; the high-frequency dynamic is completely eliminated when the voltage passes through parasitic capacitors, effectively suppressing current leakage.

On the basis of a buck–boost circuit, coupling inductance has been proposed by Ali et al. (2021) to regulate power output, forming a secondary voltage gain adjustment strategy. In order to reduce the leakage current and number of components and to improve transfer efficiency, a transformer-free converter structure based on MOSFET power switches was proposed by Dhara and Somasekhar (2022); it shares a common ground between the PV source and grid and applies a zero-beat controller instead of a PI controller. In Yari et al. (2022), a three-phase multi-level converter based on three-level neutral point clamp quasi Z-source topology was proposed to implement maximum power tracking. These methods give almost no or very little consideration for energy conversion efficiency.

In order to achieve high efficiency and negligible loss during high-frequency switching, Gao et al. (2022) proposed a buck–boost PV converter structure with six switches which operates at different frequencies under a discontinuous mode with zero current leakage. A new seven-level common ground (CG) switched capacitor (SC)-based grid-tied transformer-less converter was introduced in Husev et al. (2022) which has three times the boosting capability of input voltage. To step up the input PV voltage and facilitate seven steps in output voltage, two SC cells are connected in parallel.

Inspired by the research outlined above, we designed a buck–boost structure and propose an effective coordinated control in DC–DC and DC–AC to improve power conversion efficiency and reduce harmonics. The configuration and operation mechanism of the PV converter with buck–boost DC links is analyzed in the second section. The third section discusses a coordinated control strategy with the current hysteresis loop on the DC–DC link and converter. To validate the superiority of the proposed coordinated control strategy with the current hysteresis loop strategy, a rigorous experimental evaluation was conducted by designing a rapid control prototype (RCP) framework which gives the simulation verification of the designed converter and the proposed coordinated control strategy, detailed in the fourth section. Conclusions are drawn in the fifth section.

2 Analysis of the structure and operating mechanism of photovoltaic converters based on a buck–boost DC link

The circuit structure of a buck–boost converter with a single photovoltaic (PV) panel is shown in Figure 1. The coordinated current hysteresis control proposed in this paper mainly controls the S1 and S2 switches of the DC link to accelerate its dynamic response ability; these are independently controlled with the converter switches S3–S8. The rationality of the switch control design in the DC–DC link directly affects the quality of the voltage output by the converter. Therefore, the focus here is on the switch control of the DC–DC link while ensuring that the converter switch is normally turned on or off.

The current hysteresis control belongs to PWM (pulse width modulation) tracking technology, the basic idea of which is to compare the controlled variable (usually including the output voltage or the inductor current in the DC–DC link) with its given value. If the difference between the controlled variable and its given value is greater than the set upper limit value, the switch state is changed to reduce the controlled variable. If their difference is less than a set lower limit value, the switch state is changed to increase the controlled quantity. If their difference is between the lower and upper limits, the switch will be kept on. Therefore, the current hysteresis control belongs to the closed-loop control, which has the characteristics of real-time control and fast response speed. Moreover, by changing the upper and lower limits of error, tracking accuracy can be easily controlled. In fact, the current hysteresis control is a non-linear control that can significantly improve the non-linear dynamic performance of the converter. Considering that

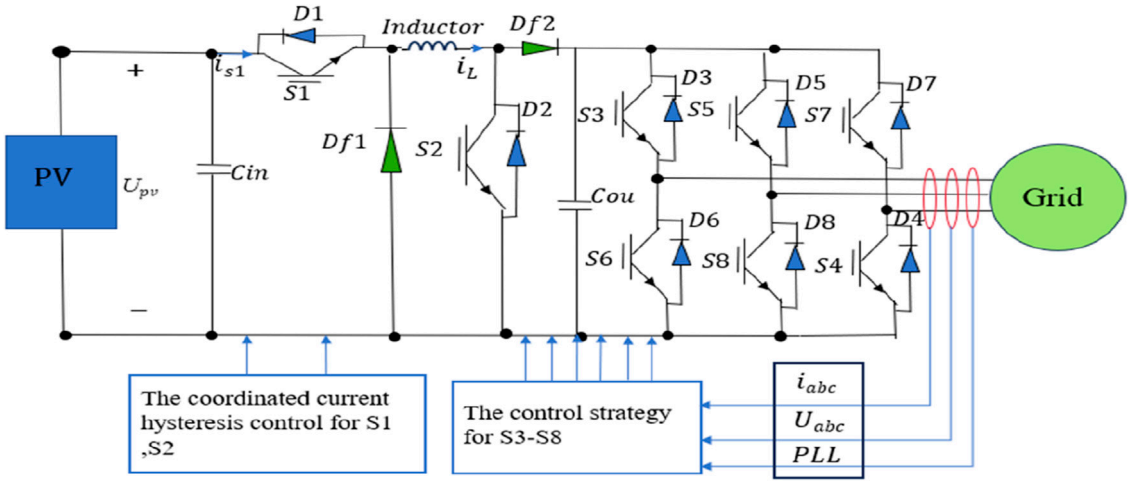

FIGURE 1
Circuit structure of the buck–boost converter with a single photovoltaic panel.

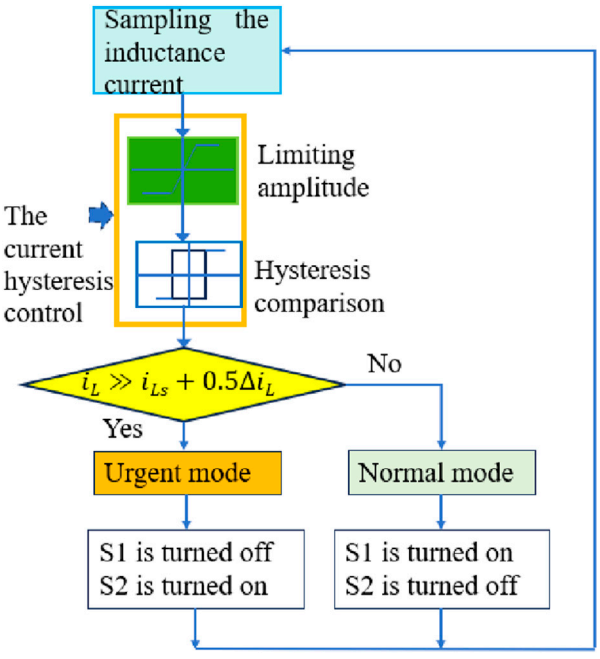

FIGURE 2
Control flow chart of the current hysteresis control.

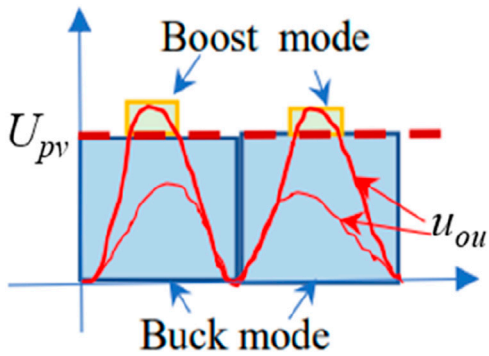

FIGURE 3
Buck and boost mode discrimination.

the PV systems are easily affected by environmental factors such as sunlight, temperature, and cloud cover, the variation range of the output voltage at the PV panel is relatively wide, which can lead to large fluctuations in inductance current. Therefore, the buck–boost converter using inductance current hysteresis control is introduced to adjust the PWM output signal based on the grid current as a reference in hysteresis control, thereby adjusting the duty cycle of the high-frequency switch and adjusting the inductance current in the buck–boost DC link.

In our work, the current hysteresis control of the DC–DC link introduces a current deviation detection loop comprising a limiting loop and a hysteresis comparison loop. Introducing the two loops creates a relationship between output voltage, output current, and inductor current, forming the current hysteresis control strategy based on the changes in output voltage, current, and inductor current to coordinate the on/off modes of S1 and S2 and limit the amplitude of the inductor ripple current. By using the current hysteresis control, sudden changes in input voltage will not have any impact on the average output voltage, only on ripple. Here, current hysteresis control is introduced. The control flow chart of the current hysteresis control is shown as Figure 2. When the transient current of the inductor exceeds a certain range $i_L \geq i_0 + 0.5\Delta i_L$ (i_L is the actual value of the inductor current; i_0 is the reference value of the inductor current; Δi_L is the variation value of the inductor current) in real-time monitoring, the urgent mode current hysteresis control is started to regulate the duty ratio of the S1 and S2 switches to avoid excessive fluctuations in the inductor current. When the inductor current is within the range $i_L \leq i_0 + 0.5\Delta i_L$, it falls in the normal mode, which is the actual processing scope of the PI control.

Figure 3 shows the discrimination in the buck–boost mode. To select this mode, the corresponding switching signal needs to be

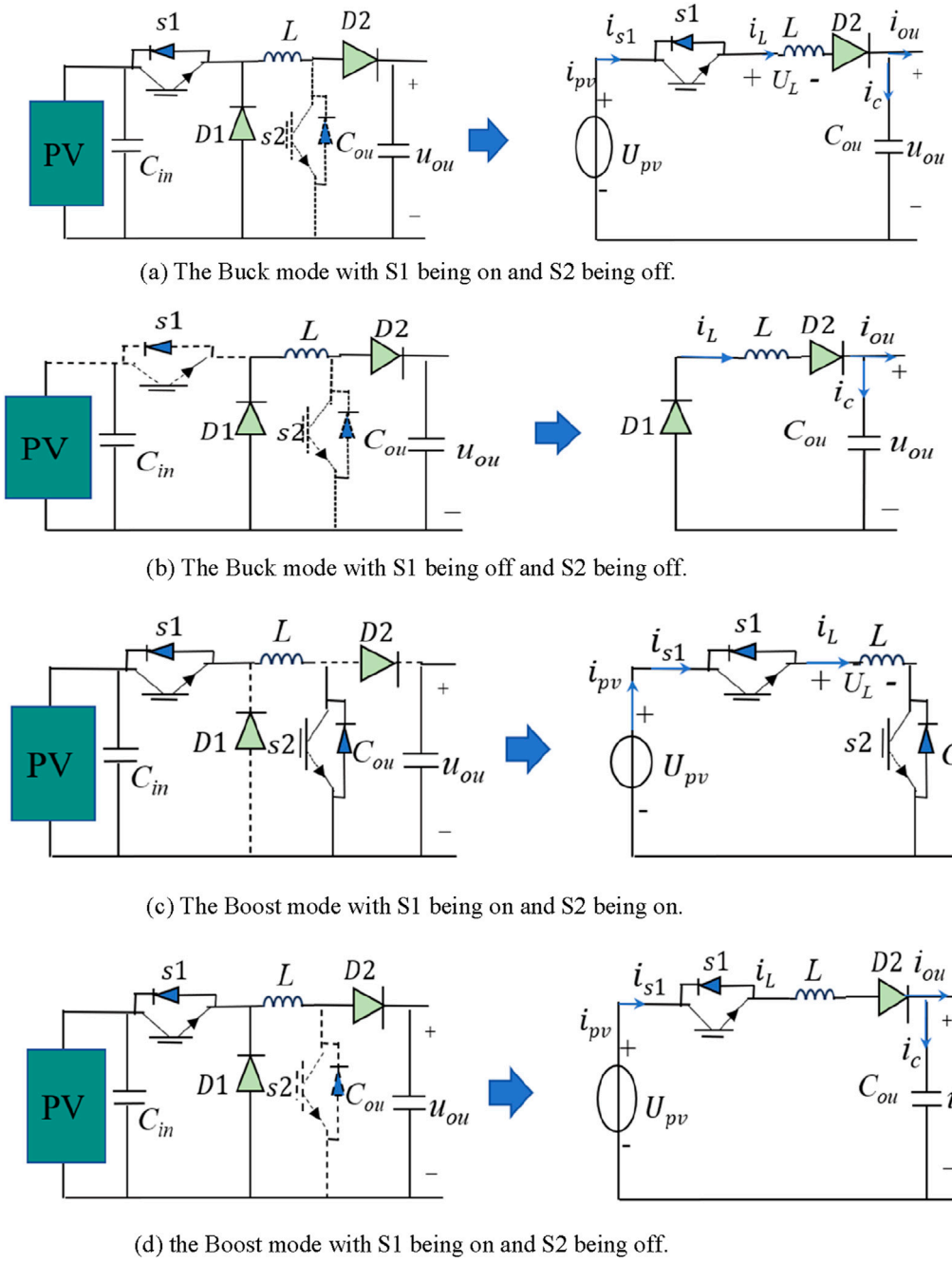

FIGURE 4
Equivalent circuit for buck and boost mode. **(A)** Buck mode with S1 on and S2 off. **(B)** Buck mode with S1 and S2 off. **(C)** Boost mode with S1 and S2 on. **(D)** Boost mode with S1 on and S2 off.

given. Determining the buck or boost mode completely depends on the comparison of the voltage of capacitor u_{cou} and the output voltage U_{PV} of the PV panel. If U_{PV} is lower than u_{cou}, it is in the buck mode, which means that the input voltage in the DC–DC link should be increased. If U_{PV} is higher than u_{cou}, it is in the boost mode, which means that the input voltage in the DC–DC link should be decreased.

According to the operating characteristics of the buck–boost converter under different operating modes, its operating mechanism is elaborated in detail as follows.

2.1 Buck mode: $u_{cou} < U_{PV}$, S1 is on, S2 is off; S1 is off, S2 is off

In Figure 4A, the voltage at the PV panel port is equivalent to the DC source U_{PV}. The voltage at the grid-tied point is assumed to be stable, and the capacitor used for voltage stabilization and connected in parallel with the PV panel is ignored. Hence, the i_{pv} current flowing out from the PV panel is equal to i_{s1}. When S1 is turned on and S2 is off, i_{s1} is also equal to i_L. The inductor is charged, and the current flowing through it not only charges the capacitor but also supplies the grid. The

voltage at both ends of the inductor is positive on the left and negative on the right, resisting the increase in current. In the PV panel, the output voltage is variable; hence, the output current i_{pv} is also variable. To maintain the output voltage of the DC link as a half wave sine, it is necessary for the S1 and S2 switches to be sinusoidal. Therefore, based on the equivalent circuit in the buck mode (Figure 4A), combined with Kirchhoff's voltage and current theorem, the voltage and current relationship of the input and output ports of the PV panel and DC–DC link can be obtained as Equations 1, 2:

$$i_{pv} = i_{s1} = i_L = i_c + i_{ou}, \tag{1}$$

$$U_{pv} = U_L + u_{cou}. \tag{2}$$

According to Equation 2 the relationship between inductance current and voltage can be represented as Equation 3.

$$U_{pv} = L\frac{di_L}{dt} + u_{cou}. \tag{3}$$

According to Equation 3, further deformation can be carried out to obtain Equation 4.

$$\Delta i_L = \frac{U_{pv} - u_{cou}}{L}\Delta t_1, \tag{4}$$

where Δi_L is the inductor current variation value, Δt_1 is the time of switch being on. $\Delta t_1 = d_1 T$, where d_1 is the duty cycle of the sinusoidal variation of S1 and T is the work period. d_1 is expressed as

$$d_1 = \frac{u_{cou}}{U_{pv}}, \tag{5}$$

where d_1 is the ideal duty cycle of S1. The triggering pulse of S1 synchronizes with the phase change of the U_g voltage at the grid-tied point, which not only ensures that the capacitor voltage u_{cou} is consistent with the grid but also ensures that the voltage waveform is a standard sine waveform. Hence, the duty cycle of S1 shown as Equation 5 is modified as

$$d_1 = \frac{u_{cou}}{U_{pv}} + \rho\Delta i_L, \tag{6}$$

where $\rho = \frac{L}{TU_{pv}}$; i_L is the actual value of inductance current. In Equation 6 when ρ remains constant, the increased Δi_L implies that the actual value of the inductance current should be decreased. The maximum power point voltage U_{PV} tracked by MPPT should be decreased, and d_1 should be decreased. If Δi_L decreases, the actual value of the inductor current should be increased. Hence, the maximum power point voltage U_{PV} tracked by MPPT should be increased and d_1 should be increased. Adjusting the duty cycle expression in real-time ensures that the output voltage can still be maintained at a relatively stable level even when the voltage at the PV panel port changes. After obtaining the expression for the duty cycle, Δi_L can be further expressed as

$$\Delta i_L = \frac{U_{pv} - u_{cou}}{L} \cdot d_1 \cdot T. \tag{7}$$

Let setting $\Delta U_{pv} = U_{pv} - u_{cou}$. ΔU_{PV} includes the fluctuation of the PV panel port voltage and its impact on the capacitor output voltage, as the fluctuation of capacitor output voltage is caused by improper control in buck mode. Equation 7 can be further expressed as Equation 8.

$$\Delta i_L = \frac{\Delta U_{pv}}{L} \cdot d_1 \cdot T. \tag{8}$$

The average current passing through S1 in one switching cycle is Equation 9.

$$i_{s1\_T} = d_1 \cdot i_{ou}. \tag{9}$$

When the driving signal of switch S1 is turned to a low level, the switch is turned off, and the inductor L is discharged through the freewheeling diode $D1$. The inductor current gradually decreases, and the inductor voltage reverses to resist the decrease in inductor current. The output voltage is maintained by the discharge of the capacitor C_{ou} and the reduced inductor current. The equivalent circuit is shown in Figure 4B. The output voltage of C_{ou} and the current variation of inductor is expressed as Equations 10, 11.

$$L\frac{di_L}{dt} = u_{cou}, \tag{10}$$

$$\Delta i_L = \frac{u_{cou}}{L}\Delta t. \tag{11}$$

When S1 is turned off, the inductor is discharged until S1 and S2 turn on again.

2.2 Boost mode: $u_{cou} > U_{PV}$, S1 turns on, S2 turns on; S1 turns on, S2 turns off;

According to the equivalent circuit of the boost mode with S1 and S2 both on (Figure 4C) with $u_{cou} > U_{PV}$, inductor L is charged again and the capacitor is discharged to keep the output voltage. The relationship between the port voltage of the PV panel and the inductor current is

$$U_{pv} = L\frac{di_L}{dt}. \tag{12}$$

According to Equation 12, the change of the inductor current is calculated as Equation 13.

$$\Delta i_L = \frac{U_{pv}}{L}\Delta t_2, \tag{13}$$

where Δt_2 is the turning-on time of S2. Considering $\Delta t_2 = T\left(1 - \frac{1}{d_1}\right)$, Δi_L can also be calculated as Equation 14.

$$\Delta i_L = \frac{U_{pv}}{L}T\left(1 - \frac{U_{pv}}{u_{cou}}\right). \tag{14}$$

When S1 turns on and S2 turns off, the equivalent circuit is shown in Figure 4D, which is the same as Figure 4A. The inductor is continuously charged, and the capacitor also starts to be charged after discharging for $d_2 T$. The analysis process is the same as in Figure 4A. Additionally, the voltage and current at the grid-tied point with the converter are set as U_g and I_g, which are both the RMS of u_g and i_g. The amplitude of the output voltage u_{cou} of the capacitor is U_{coum}. The active power generated by the PV panel is expressed as

$$\begin{aligned} P_g &= \frac{1}{\pi}\int_0^{\pi} p_g d(\omega t) \\ &= \frac{2}{\pi}\int_0^{\pi} u_{cou} i_g d(\omega t). \end{aligned} \tag{15}$$

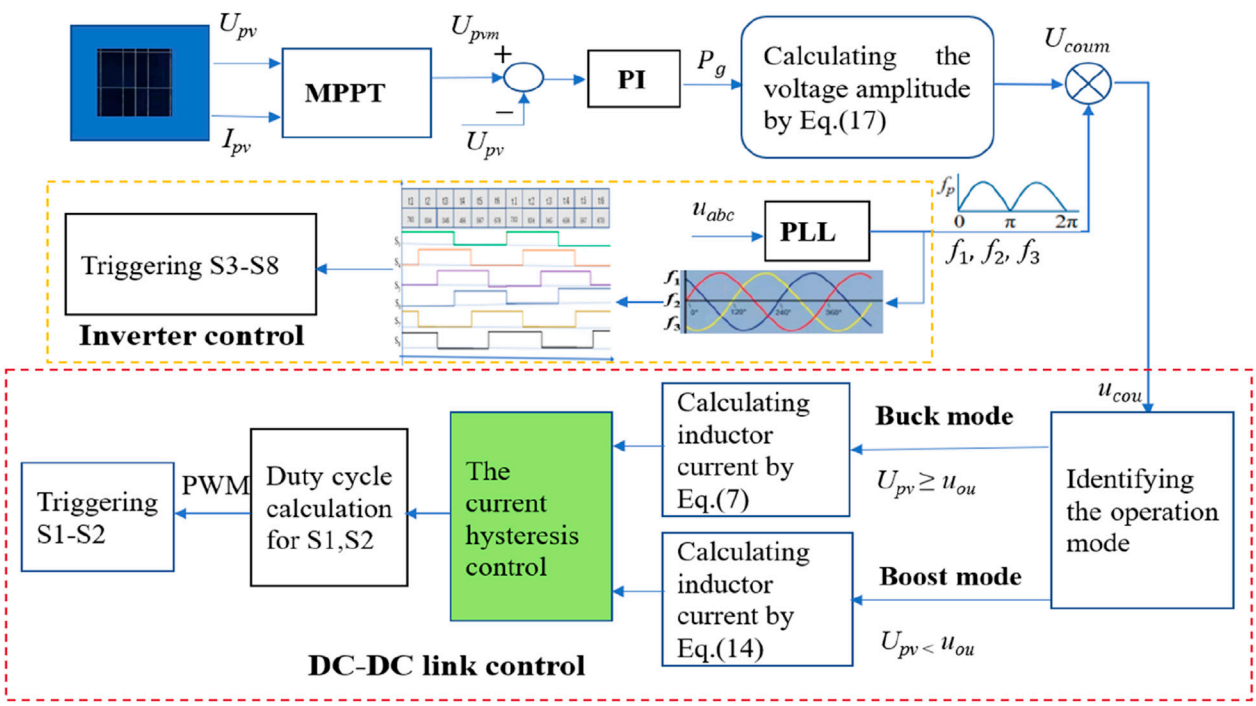

FIGURE 5
Block diagram of the coordinated control method for the whole PV converter.

Because u_{cou} is synchronized with the grid-tied voltage u_g, Equation 15 can be expressed as Equation 16.

$$P_g = \frac{2}{\pi}\int_0^{\pi} U_{coum}\sin(\omega t)\sqrt{2}I_g\sin(\omega t)d(\omega t) = \sqrt{2}U_{coum}I_g. \quad (16)$$

Then, the capacitor voltage amplitude of the DC–DC link can be calculated as Equation 17.

$$U_{oum} = \frac{P_g}{\sqrt{2}I_g}. \quad (17)$$

The voltage amplitude of the capacitor is calculated to perform the operation mode discrimination for buck or boost mode in the coordinated control algorithm with the current hysteresis loop.

3 DC–DC coordinated control strategy with the current hysteresis loop

When the insolation changes, U_{PV} changes correspondingly. If the switch sequence and duty cycles are still operated at the determined mode, the output voltage does not remain constant. To maintain a constant output voltage, the controller must track the voltage changes in the PV panel and adjust the switch sequence and duty cycle in real time based on the changes in voltage changes. Therefore, a coordinated control method for the whole PV converter is proposed; its block diagram is shown in Figure 5.

The whole control diagram includes the converter control and DC–DC link control. In the converter control, the phase-locked loop (PLL) samples the three-phase voltage at the grid side to obtain the three-phase voltage waveform of the grid as f_1, f_2, and f_3, based on the triggering pulse sequences and duty cycles of the S3–S8 switches of the converter. In the DC–DC link control, the MPPT module collects the U_{pv} voltage and I_{pv} current of the PV panel and tracks the maximal power point U_{pvm}. The difference between U_{pvm} and the actual value U_{pv} is processed by the PI controller to generate the active power P_g, which is needed for calculating the voltage amplitude U_{coum} of the expected output voltage of the capacitor. The expected output voltage u_{cou} is then obtained by multiplying the voltage amplitude U_{coum} with the f_p from the PLL, which is obtained by the frequency-based replacement. The expected voltage u_{cou} is compared with U_{PV} in the discriminating operation mode module to determine the buck or boost mode. According to different operation modes, the calculation methods for inductor current changes Δi_L are different. Under the buck mode, the inductor current change is calculated by Equation 7, which is used to modify the duty cycle for S1, while in boost mode, the inductor current change is calculated by Equation 14, which is used to modify the duty cycle for S2. Considering that the changing range of the inductor current is wide, the amplitude limitation and hysteresis comparison loops are used to decrease the inductor current ripple. S1 and S2 are the high frequency switches. The PWM (pulse width modulation) technique is applied to control S1 and S2.

To maintain a constant output voltage, the converter control needs to track the voltage changes in the grid-tied point and adjust the switch sequence of S3–S8. To obtain the three-phase sinusoidal voltage at the terminal of the converter, the S3–S8 switches of the converter must follow a certain triggering sequence and duration to

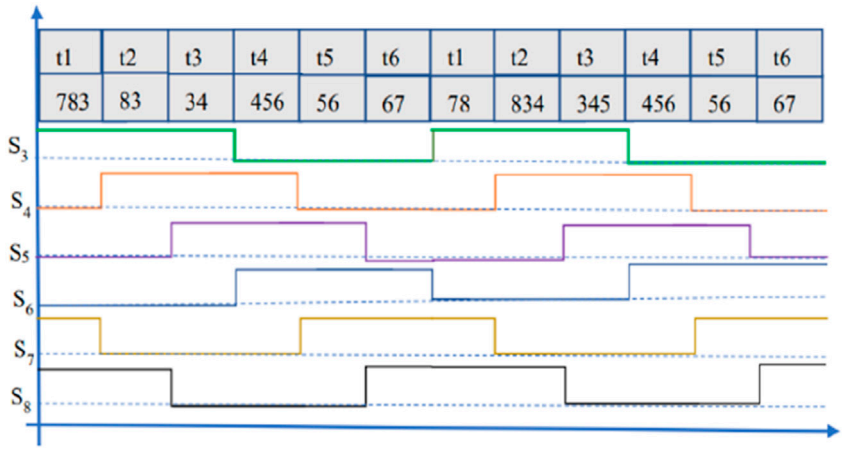

FIGURE 6
Trigger timing sequence and duty cycle length of S3–S8.

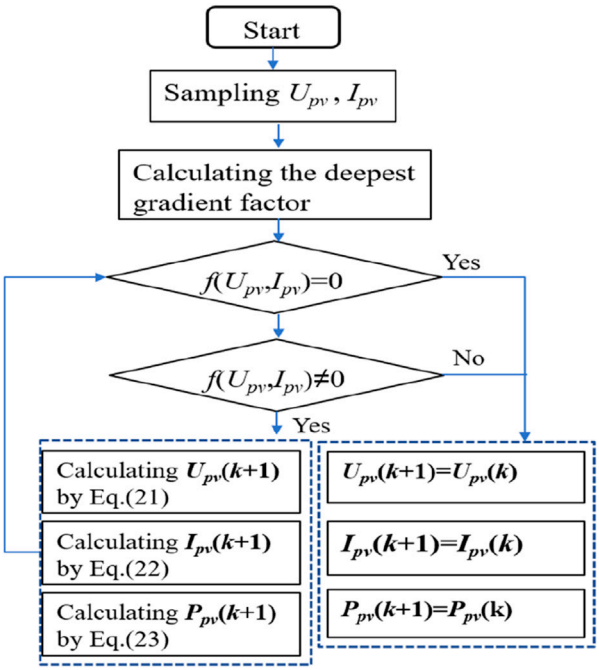

FIGURE 7
Maximum power point search algorithm based on steepest gradient descent.

TABLE 1 Parameter of photovoltaic converter with buck–boost.

Element	Specific parameter
$U_{abc}f_g$	380 V,50 Hz
L,L_g,C_{ou}	0.5 mH,0.4 mH,4 μF
Ground capacitor	0.1 μF
S1–S2 switch frequency	50 kHz
S3–S8 switch frequency	15 kHz
MPPT algorithm	Incremental conductance method based on the fastest gradient
IGBT (s1-s8)	FGA25N120ANTD
Diode (D1-D2)	MBR40250
DSP	TMS320F28335

maintain synchronization with the voltage of the grid-tied point. Figure 6 shows the designed triggering sequence for S3–S8.

The maximal power point tracking algorithm in the MPPT module for the PV system includes the incremental conductance method (INC) and the perturb and observe algorithm (P&O). P&O belongs to the local search algorithms and is susceptible to noise and shadow interference. Compared with P&O, INC shows a fast response but is prone to impact by the step size and sampling frequency.

Therefore, the steepest gradient factor is combined to improve the search speed of the maximal power point. As shown in Figure 7, the first step is to determine the gradient factor, so the steepest gradient factor expression is set as Equation 18.

$$f\left(U_{pv}, I_{pv}\right) = \frac{dI_{pv}}{dU_{pv}} + \frac{I_{pv}}{U_{pv}}. \tag{18}$$

$f\left(U_{pv}, I_{pv}\right)$ will change within the range (-1,+1) with the change of operation point of the PV system, showing the gradient change characteristic. Compared with the traditional INC algorithm, gradient factor $f\left(U_{pv}, I_{pv}\right)$ is actually a direction search factor whose value (negative or positive) shows the searching direction for the maximal power point. In this paper, the gradient factor is introduced into the calculation of U_{PV}, I_{PV}, and P_{PV} at the $(k+1)^{th}$ time. The maximal power point searching equation is shown as

TABLE 2 Changes in voltage, current, and power parameters of photovoltaic panels under different insolations.

Time(s)	0	2	4	6	8	10	12
Insolation on PV	0.15	0.35	0.4	0.5	0.6	0.75	0.9
Temperature of PV (°C)	20	21	23	25	27	29	31
P_{PV}/W	575	1,243	1,425	2,165	2,840	3,678	4,210
I_{gm}/A	1.2	2.8	3.2	4.0	4.9	6.0	7.3
U_{coum}/V	376	385	390	405	416	427	438
i_{Lm}/A	0.06	0.14	0.18	0.20	0.26	0.37	0.45

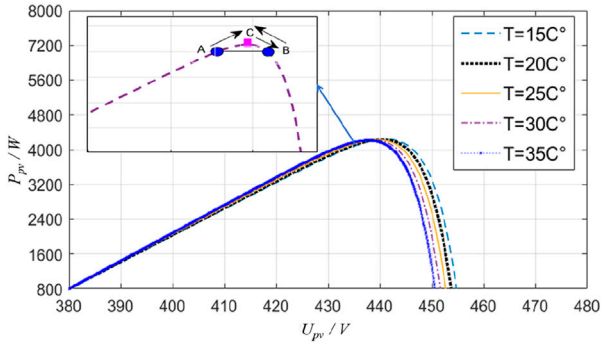

FIGURE 8
Simulated PV curves under different temperatures.

$$U_{pv}(k+1) = U_{pv}(k) + f\left(U_{pv}(k), I_{pv}(k)\right)\frac{U_{pv}(k) + U_{pv}(k-1)}{2}, \tag{19}$$

$$I_{pv}(k+1) = I_{pv}(k) + f\left(U_{pv}(k), I_{pv}(k)\right)\frac{I_{pv}(k) + I_{pv}(k-1)}{2}, \tag{20}$$

$$P_{pv}(k+1) = P_{pv}(k) + f\left(U_{pv}(k), I_{pv}(k)\right)\frac{P_{pv}(k) + P_{pv}(k-1)}{2}, \tag{21}$$

where k+1, k, and k-1 are the sampling time. U_{PV}, I_{pv}, and P_{pv} at the (k+1) time are predicted by the averaging of the k^{th} and $(k+1)^{th}$ times. Equations 19–21 are the adaptive search process, and the value of the gradient factor determines the search step size. The larger the value of the gradient factor, the shorter the search time. However, if the step size is too large, it will cause the search to exceed the limitation, and *vice versa*, it will affect the extension of the search time. Therefore, the second term in Equations 19–21 is to average the sampling values at k and k-1, and appropriately reduce the search step size.

4 Simulation and experimental verification

To verify the practicability of grid-tied PV system operation for the proposed buck–boost structure and the coordinated control strategy with the current hysteresis loop, the component parameters are set as per Table 1. The HNZL DC power supply has been used to imitate the effect of insolation. In order to emulate simultaneous variation in temperature and in the level of insolation, the MPP parameters are set as follows: U_{PV} = 400 V, I_{pv} = 6.5 A. The effectiveness verification results of the operating characteristics of the proposed converter are shown in Table 2, in which the insolation level is varied on PV. Table 2 provides the estimated mean values of i_L, P_{pv}, u_{cou}, and I_{gm}, as well as the inductance current i_{Lm} during the entire operation period. The calculation results of peak values (i_{Lm}) for P_{pv} and other states I_{gm}, U_{coum} are also presented in Table 2. The estimated values of the above quantities listed in Table 2 are consistent with the values obtained through simulation, ensuring the feasibility of the proposed method.

Figure 8 shows the relationship of the active power output and the voltage changes by the PV curves under different temperatures. When the temperature is lower, the power emitted is greater for the PV panel with the PV panel voltage being improved. When the voltage reaches 438 V, the active power output of the PV panel reaches the maximum point at 30 °C, which is consistent with the estimated value. During the MPPT process of this experiment, the maximum power point search algorithm based on steepest gradient descent takes only 0.22s to reach the maximum power point C, which is shorter than the common incremental conductance method, which is 0.31s to reach point C. This is because the improved maximum power point search algorithm based on the steepest gradient descent only searches the process from points A to C, avoiding the searching process from C to B and B to C, which saves search time. However, the common incremental conductance method tends to search from A to C, C to B, and B to C.

Figures 9A–C show the simulated changes in U_{PV}, i_{pv}, and P_{pv} of the PV panel operation states, which also demonstrate the ability of the proposed converter to operate simultaneously on the MPPT of the PV panel. Figure 10 shows the change caparison of u_{cou}, i_{s1}, i_L, and P_{pv} of the DC–DC link operation at 20 °C and 30 °C. The voltage and current curve at the PV grid-tied points at 20 °C and 30 °C with changed insolation. This shows that when the insulation varies, the voltage and current from the converter output stabilize the sinusoidal waveform synchronized with the power grid, while the current amplitude injected at the grid-collected point varies with the insolation.

Figure 11 shows the simulated voltage and current curve at the PV grid-collection points at 30 °C with changed insolation. This shows that the insolation will impact the output power of the converter. When the insolation becomes strong, the output

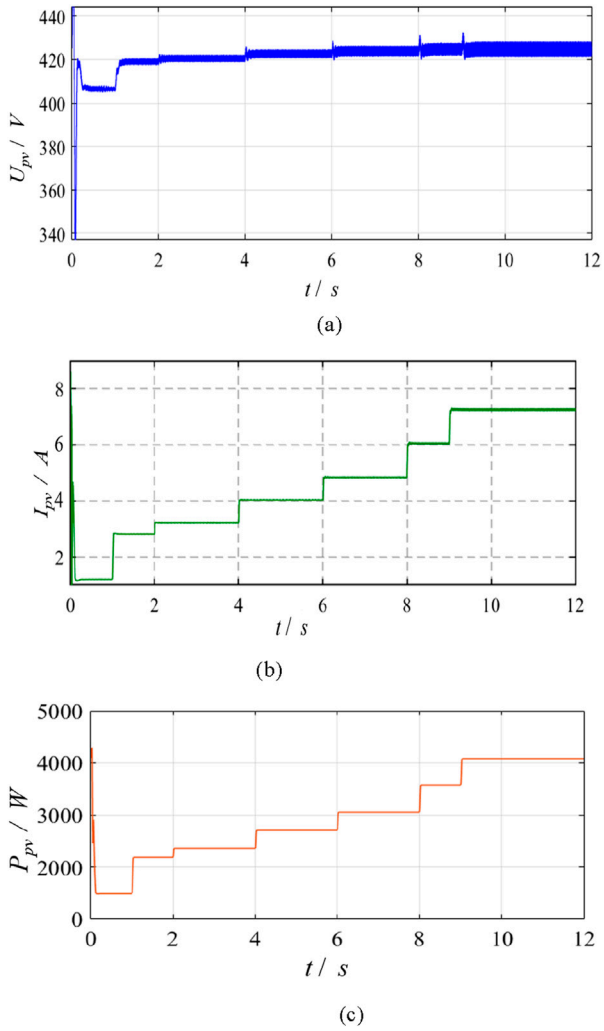

FIGURE 9
Simulated PV panel port states under different insolations: **(A)** voltage U_{PV}; **(B)** current i_{pv}; **(C)** output active power P_{pv}.

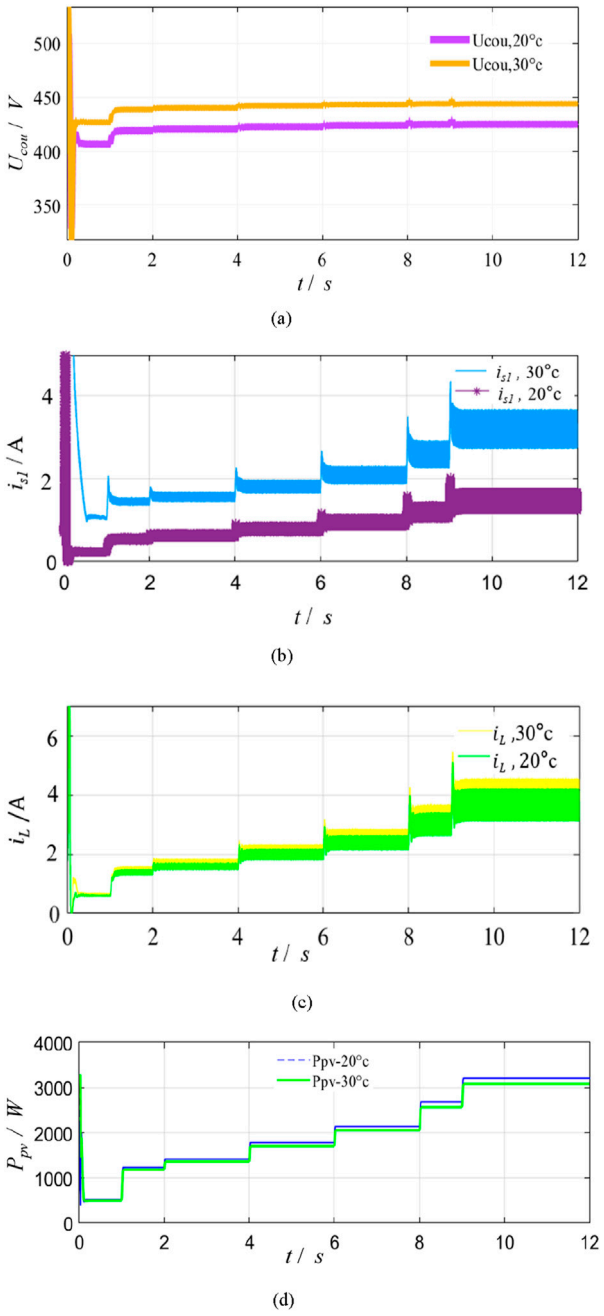

FIGURE 10
Simulated DC–DC link state curves under different temperatures: **(A)** voltage u_{cou}; **(B)** switch S1 current i_{s1}; **(C)** inductor current i_L; **(D)** output active power P_{pv}.

current of the converter increases, while the voltage of the converter remains stable; hence, the output power of the converter increases at the same time. Figure 12 compares the inductor current change when the current hysteresis control is introduced in the coordinated control under the same insolation. During the dynamic process, the ripple current of the inductor is controlled at a relatively satisfactory level, demonstrating the effectiveness of the introduced current hysteresis control. The power conversion efficiency of the PV panel is the percentage of the injected power at the grid-connection point to the output power of the PV panel. The referred voltage and current from the PV panel and grid-tied point are all at the averaging value. Figure 13 is the prototype of the designed buck–boost converter. Under the condition of the converter being off-grid, the experimental waveforms for U_g and i_g are shown in Figure 14, in which, when the input voltage of DC–DC changes from 50 V to 100 V, u_{cou} changes from 100 to 180 V and maintains a stable state. The output voltage amplitude U_g of the converter changes from 150 V to 220 V. During the whole process, the system can effectively ride through situations that arise due to the disturbances in U_g and demonstrates relatively good operation despite it experiencing significant voltage fluctuations.

Figure 15 shows the comparison results between the actual and estimated conversion efficiency of the PV converters, from which it can be inferred that the estimated value tends to consider the ideal situation and ignore the actual ambient condition, resulting in overestimated efficiency. At the maximal power point of 700 W, the actual conversion efficiency is just 97.8%, lower than the

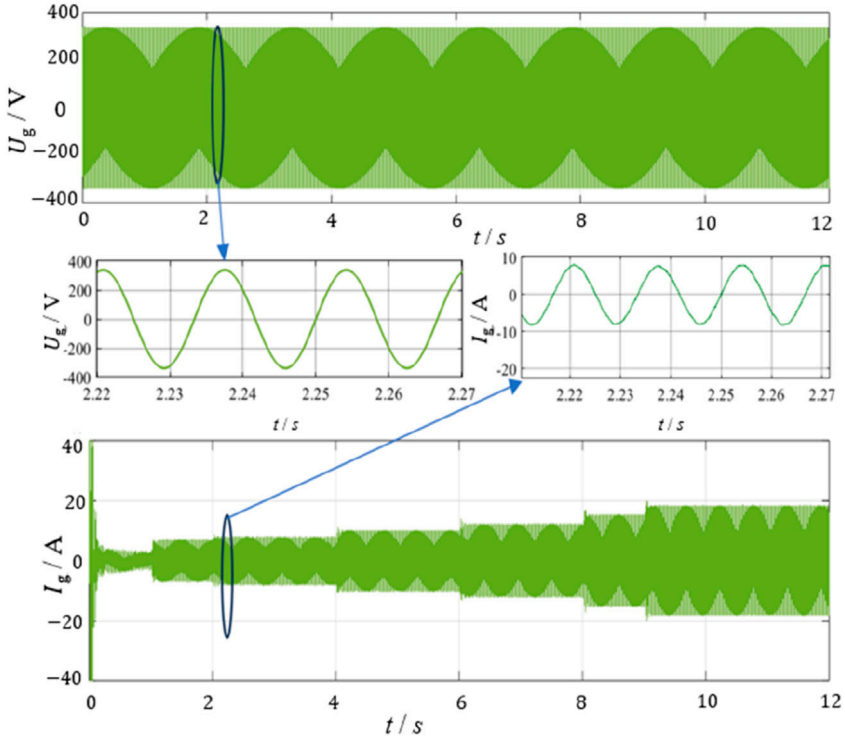

FIGURE 11
Simulated voltage and current curve at photovoltaic grid-collection points at 30 °C with changed insolation.

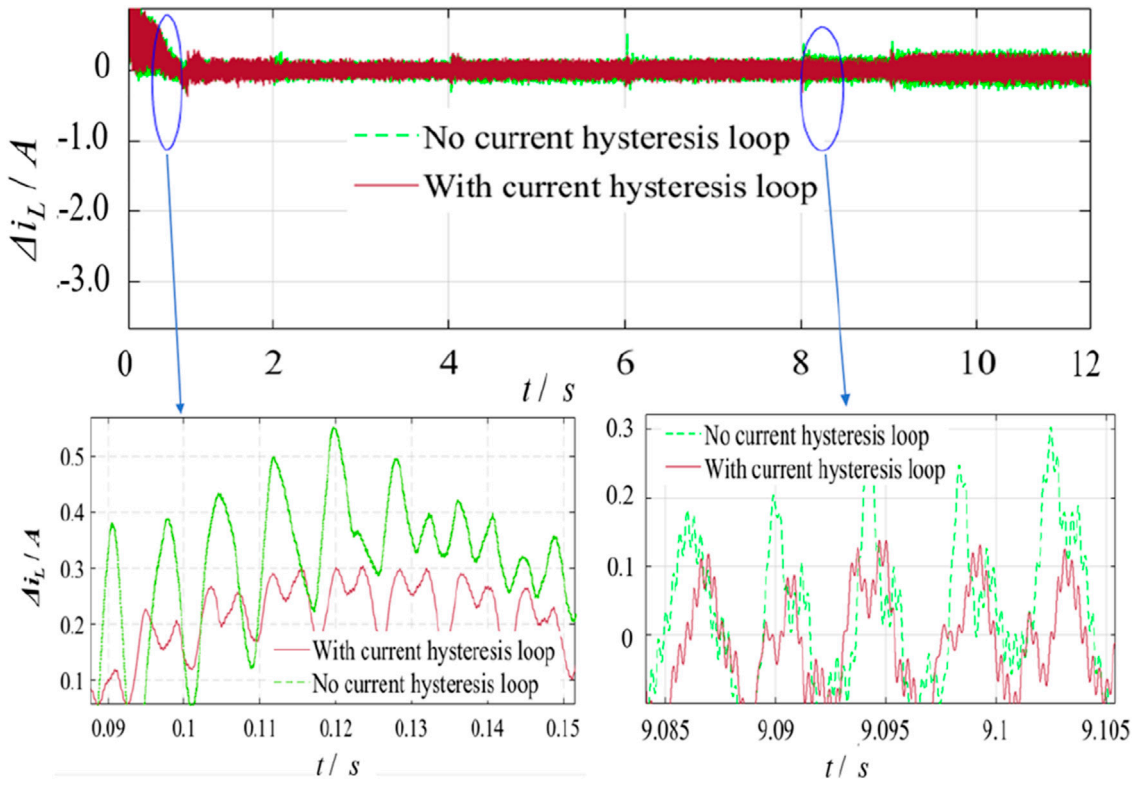

FIGURE 12
Simulated inductor current suppression comparison under same insolation.

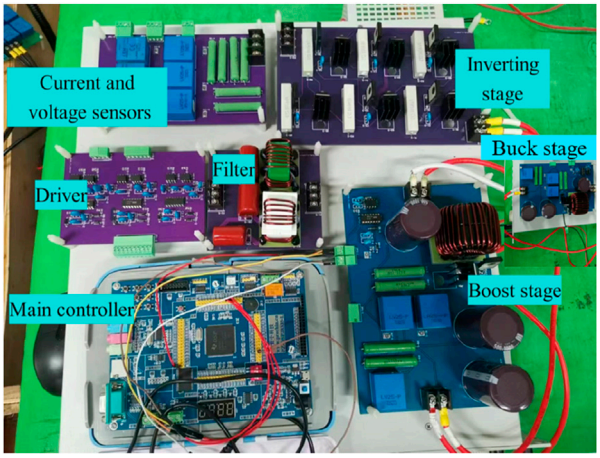

FIGURE 13
Prototype of the designed buck–boost converter.

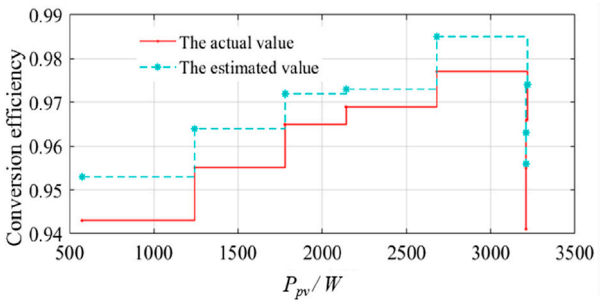

FIGURE 15
Comparison curve between the actual conversion efficiency and estimated conversion efficiency of photovoltaic converters.

estimated value of 98.7%. To further assess the impact of the current hysteresis loop on conversion efficiency, those efficiencies with current hysteresis and without hysteresis are calculated. Figure 16 shows that during the period of low power output, the conversion efficiency with the current hysteresis loop is almost the same as that without current hysteresis loop control. However, with the active power output of the PV panel increasing, the conversion efficiency considering the current hysteresis loop decreases. This means that the increasing active power output corresponds to the increasing inductor current, which is suppressed by the current hysteresis loop at the cost of conversion efficiency. Figure 17 shows the THD comparison curves between the method in Dutta and Chatterjee (2018) and the proposed method here. According to the datum, the changing trend of the THD in the grid-tied point with the output voltage increase of the PV panel remains consistent in the two methods. However, the THD in the proposed method is lower than in Dutta and Chatterjee (2018). Furthermore, the voltage variation range dealt by the method proposed here is 120 V–600 V, with a wider

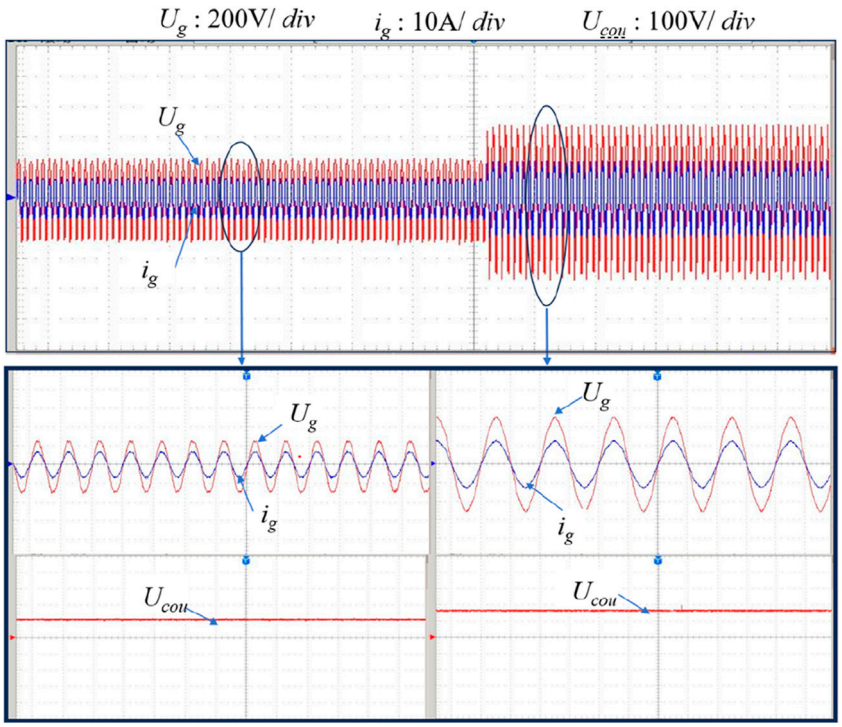

FIGURE 14
Experimental waveforms for U_g, i_g, and u_{cou}.

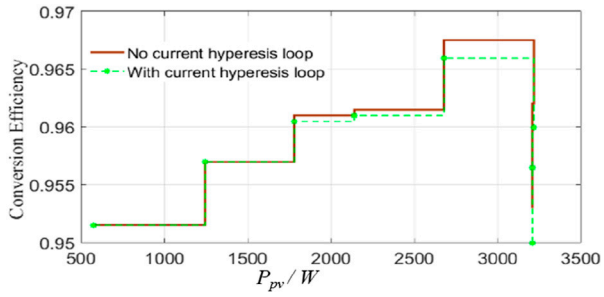

FIGURE 16
Comparison of the conversion efficiency between photovoltaic panels with or without current hysteresis.

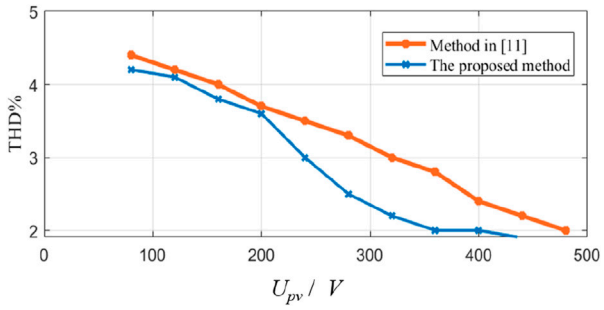

FIGURE 17
Comparison of the THD ratio of the method in Dutta and Chatterjee (2018) and the method proposed here.

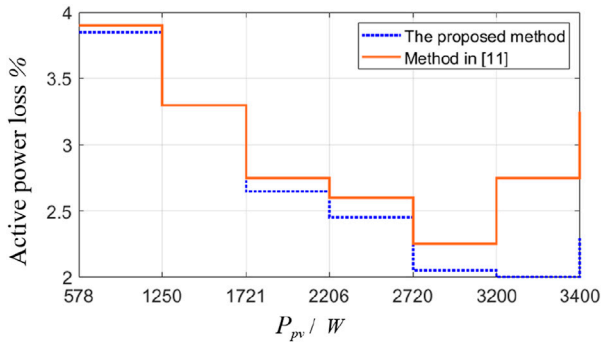

FIGURE 18
Loss distribution at different power levels.

variation range than that in Dutta and Chatterjee (2018). The active power losses at different power levels are also calculated (Figure 18). The comparison results imply that the active power loss values in our method and in Dutta and Chatterjee (2018) are almost the same when the output power of the PV panel is below 1,700 W. Then, with the output power of the PV panel increasing, the active power loss in Dutta and Chatterjee (2018) is higher than the method proposed here, especially when the output power is more than 3,200 W. This shows that the designed converter can adopt higher power production. The above results verify that the designed buck–boost PV converter with the coordinated control strategy has improved operational performance.

5 Conclusion

A buck–boost converter structure and corresponding coordinated control strategy is designed for a grid-tied photovoltaic (PV) panel in this paper. By simulation and experimental verification, the following conclusions are drawn.

(1) To improve the robustness and easing the requirement for PWM dead-times, a wide range buck–boost operation for large fluctuations in PV voltage is provided, and large buck–boost inversions are obtained with relatively smaller duty ratios. Through the operational performance comparison with the classical buck–boost converter, the buck and boost stages in the DC–DC link are decoupled and controlled separately through two switches, which is beneficial for expanding the voltage conversion range of the DC–DC link. However, the designed converter can withstand overlap time in complementary switches without voltage shoot-through problems. At the same time, the incremental conductance method is improved by introducing the deepest gradient factor, which improves the search speed of the maximum power point and enhances the dynamic performance of the converter.

(2) Considering the significant fluctuation of inductor current in the boost stage, a DC–DC coordinated control scheme based on current hysteresis control is here proposed. Based on traditional duty cycle calculation, the influence of the inductor current is introduced, and a duty cycle adjustment based on the current hysteresis control is performed to reduce the ripple of the inductor current at the cost of reducing the conversion efficiency of the PV converter. However, by comparison with the classical buck–boost converter, the designed converter shows noticeable improvement in the THD ratio with the input voltage increase of the DC–DC link. Furthermore, the active power loss caused by the designed converter is also reduced by the coordinated control strategy.

However, under conditions of partial shading, the efficiency of the designed converter is still greatly decreased, the reduction depending on the size of the shading area. The PV ground leakage current is still another unsolved problem in our scheme. Further research should focus on diminishing the leakage current, improving the power conversion efficiency of multiple PV panel series, and suppressing common mode currents under

voltage imbalance caused by different insolation conditions and shadowing.

Data availability statement

The original contributions presented in the study are included in the article/supplementary material; further inquiries can be directed to the corresponding author.

Author contributions

ZC: writing–review and editing, conceptualization, investigation, and methodology. ZH: conceptualization, project administration, resources, and writing–original draft. JA: conceptualization, methodology, visualization, and writing–review and editing. WF: visualization, data curation, investigation, and writing–original draft. YH: visualization, writing–review and editing, and methodology. QL: writing–review and editing, writing–original draft, and conceptualization.

Funding

The authors declare that financial support was received for the research, authorship, and/or publication of this article. This paper is supported by the project of Economic Research Institute of State Grid Hebei Electric Power Co., Ltd., grant number is SGHEJY00GHJS2310078.

Conflict of interest

Authors ZC, ZH, JA, WF and YH were employed by State Grid Hebei Electric Power Co., Ltd.

The remaining author declares that the research was conducted in the absence of any commercial or financial relationships that could be construed as a potential conflict of interest.

The authors declare that this study received funding from Economic and Technical Research Institute of State Grid Hebei Electric Power Co., Ltd. The funder had the following involvement in the study: collection, analysis, interpretation of data.

Publisher's note

References

Ali, M., Padmanaban, S., Ramachandaramurthy, V. K., MitoloO, M., and Benbouzida, M. (2021). A novel solar photovoltaic fed TransZSI-DVR for power quality improvement of grid-connected PV systems. *IEEE Access:Special Sect. Evol. Technol. Energy Storage Syst. Energy Syst. Appl.* 9, 7263–7279. doi:10.1109/access.2020.3048022

Alluhaybi, K., Batarseh, I., Hu, H., and Chen, X. (2020). Comprehensive review and comparison of single-phase grid-tied photovoltaic microinverters. *IEEE J. Emerg. Sel. Top. Power Electron.* 8 (2), 1310–1329. doi:10.1109/jestpe.2019.2900413

Arup, R. P., Bhattacharya, A., and Chatterjee, K. (2023). A single-phase grid-connected boost/buck–boost-derived solar PV micro-inverter topology having power decoupling capability. *IEEE J. Emerg. Sel. Top. Power Electron.* 11 (2), 2340–2349. doi:10.1109/jestpe.2023.3234070

Callegaro, L., Ciobotaru, M., Pagano, D. J., and Fletcher, J. E. (2019). Feedback linearization control in photovoltaic module integrated converters. *IEEE Trans. Power Electron.* 34 (7), 6876–6889. doi:10.1109/tpel.2018.2872677

Chauhan, S., Singh, B., and Singh, B. (2021). Control of three-phase grid integrated multiple solar photovoltaic arrays-BES based MG. *IEEE Trans. Industry Appl.* 57 (6), 6167–6181. doi:10.1109/tia.2021.3109843

Dhara, S., and Somasekhar, V. T. (2022). A three-phase semi-single stage PV inverter with voltage boosting and leakage current minimization. *IEEE Trans. Circuits Systems—II Express Briefs* 69 (1), 169–173. doi:10.1109/tcsii.2021.3082580

Dutta, S., and Chatterjee, K. (2018). A Buck and boost based grid connected PV inverter maximizing power yield from two PV arrays in mismatched environmental conditions. *IEEE Trans. Industrial Electron.* 65 (7), 5561–5571. doi:10.1109/tie.2017.2774768

Dutta, S., and Chatterjee, K. (2020). A coupled inductor-based buck–boost type grid connected transformerless PV inverter having the ability to control two subarrays simultaneously. *IEEE Trans. Industrial Electron.* 67 (7), 5543–5553. doi:10.1109/tie.2019.2931512

Gao, N., Jin, Z., Wang, H., Wu, W., Koutroulis, E., Chung, H.S.-H., et al. (2022). MOSFET-Switch-Based transformerless single-phase grid-tied inverter for PV systems. *IEEE J. Emerg. Sel. Top. Power Electron.* 10 (4), 3830–3839. doi:10.1109/jestpe.2021.3064587

Hafiz, F. A., El Moursi, M. S., Zahawi, B., and Hosani, K.A. (2021). Single-phase photovoltaic inverters with common-ground and wide buck–boost voltage operation. *IEEE Trans. Industrial Inf.* 17 (12), 8275–8287. doi:10.1109/tii.2021.3066511

Ho, C., and Siu, K. (2019). Manitoba inverter—single-phase single-stage buck-boost VSI topology. *IEEE Trans. Power Electron.* 34 (4), 3445–3456. doi:10.1109/tpel.2018.2855560

Huang, Y., Liu, F., Zhuang, Y., Diao, X., Liu, Z., Pan, S., et al. (2021). Bidirectional buck-boost and series LC-based power balancing units for photovoltaic DC collection system. *IEEE J. Emerg. Sel. Top. Power Electron.* 9 (6), 6726–6738. doi:10.1109/jestpe.2021.3074575

Husev, O., Vinnikov, D., Roncero-Clemente, C., Blaabjerg, F., and Strzelecki, R. (2022). MPPT and GMPPT implementation for buck-boost mode control of quasi-Z-source inverter. *IEEE Trans. Power Electron.* 69 (11), 11348–11358. doi:10.1109/tie.2021.3125658

Khan, M. N. H., Forouzesh, M., Siwakoti, Y. P., Li, L., Kerekes, T., and Blaabjerg, F. (2020). Transformerless inverter topologies for single-phase photovoltaic systems: a comparative review. *IEEE J. Emerg. Sel. Top. Power Electron.* 8 (1), 805–835. doi:10.1109/jestpe.2019.2908672

Kumar, S., and Singh, B. (2019). Self-normalized-estimator-based control for power management in residential grid synchronized PV-BES microgrid. *IEEE Trans. Industrial Inf.* 15 (8), 4764–4774. doi:10.1109/tii.2019.2907750

Liang, W., Liu, Y., and Peng, J. (2021). A day and night operational quasi-Z source multilevel grid-tied PV power system to achieve active and reactive power control. *IEEE Trans. Power Electron.* 36 (1), 474–492. doi:10.1109/tpel.2020.3000818

Liao, C.-Y., Lin, W.-S., Chen, Y.-M., and Chou, C.-Y. (2017). A PV micro-inverter with PV current decoupling strategy. *IEEE Trans. Power Electron.* 32 (8), 6544–6557. doi:10.1109/tpel.2016.2616371

Mohammadi, M., Moghani, J. S., and Milimonfared, J. (2018). A novel dual switching frequency modulation for Z-source and quasi-Z-source inverters. *IEEE Trans. Industrial Electron.* 65 (6), 5167–5176. doi:10.1109/tie.2017.2784346

Nan, Y., Di, Y., Zhou, Z., Jiazhan, C., Daojun, C., and Xiaoming, W. (2018). Research on modelling and solution of stochastic SCUC under AC power flow constraints. *IET Generation Transm. and Distribution* 12 (15), 3618–3625. doi:10.1049/iet-gtd.2017.1845

Srivastava, A., and Seshadrinath, J. (2023). A single-phase seven-level triple boost inverter for grid-connected transformerless PV applications. *IEEE Trans. Industrial Electron.* 70 (9), 9004–9015. doi:10.1109/tie.2022.3215815

Teodorescu, R., Liserre, M., and Rodríguez, P. (2011). *Grid converters for photovoltaic and wind power systems*. New York, NY, USA: Wiley.

Yari, K., Mojallali, H., and Hamid Shahalami, S. (2022). A new coupled-inductor-based buck–boost DC–DC converter for PV applications. *IEEE Trans. Power Electron.* 37 (1), 687–699. doi:10.1109/tpel.2021.3101905